ISSN NO: 9726-001X
Volume 9 Issue 03 2021

JOURNAL OF CURRENT SCIENCE

Phase transition driven by deformation a molecular dynamics investigation of a nanostructured polycrystalline Cr Cu Fe Ni high entropy alloy

Sharanappa Koni, Poornima.K, Dr.B.H.Manjunath

Asst. Prof, Asst. Prof, Prof. & HOD

sharanukoni@gmail.com, mechpoornima@gmail.com, bhmanj@gmail.com

Department of Mechanical, Proudhadevaraya Institute of Technology, Abheraj Baldota Rd, Indiranagar, Hosapete, Karnataka-583225

Abstract

Nanostructured polycrystalline CoCrCuFeNi high entropy alloy (HEA) high-temperature tensile characteristics are elucidated in this work by use of a battery of molecular dynamics (MD) simulations. By studying nanostructures in MD simulations, including phase change and dislocation development, we were able to deduce the process by which strength decreases at high temperatures. We found that this material may be used as a structural material at high temperatures ranging from ambient temperature to 1200 ℃. The stress-strain graph shows that as the temperature of the material rises, the ultimate tensile strength and yield stress drop. While the elastic modulus drops sharply at moderately high temperatures, it drops more slowly as temperatures rise into the severe heat range. The mechanism of energetic bond creation between atoms caused by tensile stress, known as face-centered cubic (FCC)–hexagonal close-packed (HCP) phase change, was uncovered. Between the FCC→HCP phase shift and the creation of voids, it contributes competitively to the tensile characteristics from the area around the yield stress into the quasi-plastic regime. Dislocation analysis involves measuring common partial dislocations such perfect, Shockley, stair-rod, and others. Stair-rod and Shockley partial dislocations exhibit attributes that contribute to their tensile strengths. Understanding the high-temperature application of nanostructured polycrystalline CoCrCuFeNi HEA is enhanced by the findings of this work.

Keywords: High entropy alloy, CoCrCuFeNi, Tensile test, Molecular dynamics, Phase transformation, Dislocation analysis

1. Introduction

High entropy alloys (HEAs), which consist of more than five elements, possess excellent strength and ductility at harsh environments. Unlike conventional alloying ways, this is known to generate a simple solid solution structure of face-centered cubic (FCC), hexagonal close-packed (HCP), and body-centered cubic (BCC) while generating few intermetallic compounds, contrary to expectations (Yeh et al., 2004; Cantor et al., 2004).

Among them, CoCrCuFeNi is an early type of HEA, and its microstructure in bulk material has been reported to consist of a small amount of Cu-rich interdendrite in a large amount of FCC dendrite after heat treatment of 1100 ℃ (Park et al., 2015). Although the strength retention is reported till 800 ℃ by adding 0.5-mole fraction of Al, the role of Cu was confirmed to become a segregation due to high enthalpy in mixing with other elements, and its attractiveness as a high-temperature material was halved (Praveen and Kim, 2018). On the other hand, nanocrystalline (NC) HEAs are different from bulk HEAs exhibiting poor fracture resistance as the result of grain boundary (GB) segregation and formation of impurities at GBs (Sencov et al., 2011; Xiao et al., 2019). In many types of metals, including stainless steel, which is widely used as engineering metals, GB can be thought as vulnerable (Fujii et al., 2022). Minimizing defects provides superior mechanical properties than that of bulk HEAs, thereby it is expanding its applicability in micro/nano-mechanical components (Zou, 2018; Muskeri et al., 2020).

The evaluation of the fracture processes of HEAs began recently after its microstructural integrity such as elemental distribution and phase structure was confirmed. Crack initiation and propagation mechanisms of CoCrFeMnNi HEA under fatigue load have been reported as pioneer research (Suzuki et al., 2020). The fracture process of the material through the planar slip process results in deformation localization, which in turn results in multiple crack initialization. On the other hand, in the crack propagation process, it aggregates into one crack and converts to mode I cracking. In general, in the process of initializing plastic deformation, the planar slip undergoes a phase transformation process regardless of tensile and fatigue loads, so that the micro/nano structural simulation results in its crack initiation were required additionally to explore by researchers. On the other hand, under a large deformation by high strain amplitude, the plastic deformation by twining showed improved fracture characteristics due to low stacking fault energy (Shams et al., 2020). Twinning during plastic deformation could provide improved mechanical properties owing to various microstructural mechanisms. Further, fracture mechanism of alloys at high temperature is crucial, because a mixture of atomic elements and chemical compounds influences significantly elastic and plastic deformations (Suzuki et al., 2018). Plasticity-induced fracture concept gives great contribution for high temperature fracture of a variety of alloys (Suzuki et al., 2022).

Molecular dynamics (MD) simulations are very useful for understanding the deformation properties of small-scale materials (Shirasu et al., 2021; Hirano et al., 2021). In particular, it is a good approach to understand the characteristics of micro/nano mechanical materials and the dynamic deformation of microstructures due to variables of materials, deformation and temperature (Caro and Farkas, 2018; Seoane et al., 2023; Yoon et al., 2023). HEA is difficult to model with other simulation approaches due to its high configuration entropy by its complex element arrangement. On the other hand, MD not only makes this possible, but it is also beneficial in sample size from the perspective of NC-HEA's representative volume element. In this study, high temperature tensile behavior of CoCrCuFeNi HEA was studied to understand molecular view during elastic and plastic deformations. Large-scale Atomic/Molecular Massively Parallel Simulator (LAMMPS) (Plimpton, 1995) was employed to perform a series of MD simulations. The simulation results understand the mechanical characteristics and microstructure mechanisms related to the high temperature tensile deformation of nanostructured polycrystalline CoCrCuFeNi HEA.

2. Simulation methodology

Equi-atomic CoCrCuFeNi HEA was modeled to three-dimensional configuration for simulation sample. It has single FCC phase with the lattice parameter of 3.60 Å (Park et al., 2015) based on the assumption that there is no distinction between Cu-rich and lean. Initial configuration (sample size: 500 Å×250 Å×250 Å) for atomic scale simulation was created using ATOMSK open-source program (Hirel, 2015). Atoms such as Co, Cr, Cu, Fe and Ni were randomly located in sample box and the number of atoms is approximately 2.67×10^6. We employed the size of sample box and the number of atoms to describe experimental nanostructured polycrystalline CoCrCuFeNi HEA as similar as possible. Visualization was performed using OVITO software (Stukowski, 2010). Initial configurations after energy minimization are presented in Fig. 1. Figure 1 (a) is a sample shape consisting of randomly distributed elements such as (1)-Co, (2)-Cr, (3)-Cu, (4)-Fe and (5)-Ni, respectively, and Fig. 1 (b) is the modelled FCC CoCrCuFeNi HEA processed by common neighbor analysis (CNA). Figure 1 (c) shows an example of dislocation analysis conducted by dislocation extraction algorithm (DXA). In the polycrystalline samples, randomly oriented grains were constructed by Voronoi construction (Voronoi, 1908). The average diameter as grain size was 78.7 Å.

ISSN NO: 9726-001X
Volume 9 Issue 03 2021

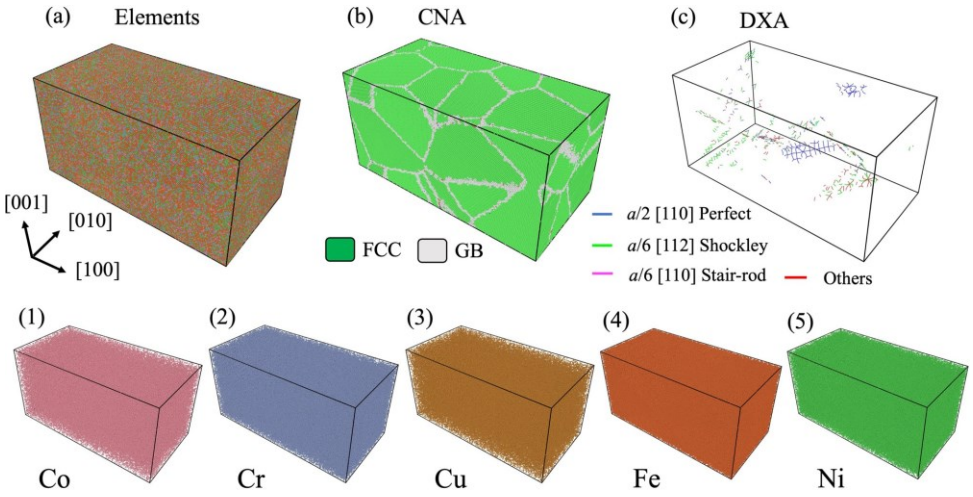

Fig. 1 Initial sample geometry of nanostructured polycrystalline CoCrCuFeNi HEA after energy minimization, (a) distribution of constituent elements, (b) polycrystal view by CNA, (c) pre-existing dislocations analyzed by DXA, and (1-5) distribution of each element.

The embedded atom method potential for CoCrCuFeNi developed by Deluigi, was applied for interatomic interactions (Deluigi et al., 2021). The interactions for the Co-Cr-Cu-Fe-Ni atoms are formerly described by $E_i = 1/2 \sum_{j \neq i} \phi(r_{ij}) + F \sum_{j \neq i} \rho(r_{ij})$. Where E_i is the potential energy of atom i. r_{ij} is the distance between the atom i and j. ϕ is the pair potential between the elements. ρ is the atomic electron density of the elements. F is the embedded energy of the elements. Before conducting a series of tensile tests, energy minimization was performed to relax the initial configuration. The sample was treated at 0.1 K without any force for 100 ps under isothermal-isobaric ensemble to enforce minimum value mean stress. Periodic boundary conditions were applied in [100], [010], and [001] directions. After these zero energetic processes, a series of tensile tests at elevated temperatures was performed. Temperature range was representatively determined between room temperature (RT) and 1200 ℃. The samples were tensioned under the following eight temperature conditions such as RT, 100, 200, 300, 400, 600, 900, and 1200 ℃ during performing each simulation. Tensile loading was applied in [100] direction with unique strain rate of 5×10^8 s^{-1}.

3. Results and discussion

3.1 Stress-strain responses at elevated temperatures

Figure 2 shows the high temperature mechanical properties of CoCrCuFeNi HEA calculated by MD simulation. Figure 2 (a) shows the engineering stress−strain ($\sigma - \varepsilon$) curve varied by the applied temperature between RT and 1200 ℃. As the temperature rises, the yield stress (YS) σ_y decreases, and the ultimate tensile strength (UTS) $\sigma_{\$T\&}$ decreases accordingly. In particular, a decrease in elastic modulus E and UTS leads to a decrease in flow stress. Measurements of mechanical properties such as σ_y, $\sigma_{\$T\&}$ and E were carried out in the elastic and quasi-plastic regimes, and those over ε of 0.45 were not considered because they correspond to fully plastic regime under the MD simulation. Like the $\sigma - \varepsilon$ curve of general alloys by MD simulation, it undergoes plastic deformation of flow stress and then is finally failured. In this study, the failure mechanism was not discussed because the mechanical properties at high temperatures were mainly interested than final failure mechanism. Figure 2 (b) shows that the high temperature mechanical properties of the material and UTS decrease linearly with increasing temperature. What is noteworthy here is plotted on the inset figure of Fig. 2 (b). Unlike other mechanical properties such as σ_y and $\sigma_{\$T\&}$, the value of E decreases nonlinearly. In general, in the case of metals, the temperature dependence of E is divided into linear or nonlinear by several parameters such as the type of material and the range of temperature (Varshni, 1970; Laplanche et al., 2015). The CoCrCuFeNi high entropy alloy studied in this paper remains linear up to a temperature of 600 ℃, but at higher temperatures, a nonlinear decrease in E appeared. In particular, it decreases rapidly to the temperature of 400-500 ℃ and then gradually decreases at the higher temperatures. This can be explained physically by the nonlinearity of microstructural changes at high temperatures. Therefore, we mainly dealt with in this study how these mechanical properties are reduced microstructurally.

ISSN NO: 9726-001X
Volume 9 Issue 03 2021

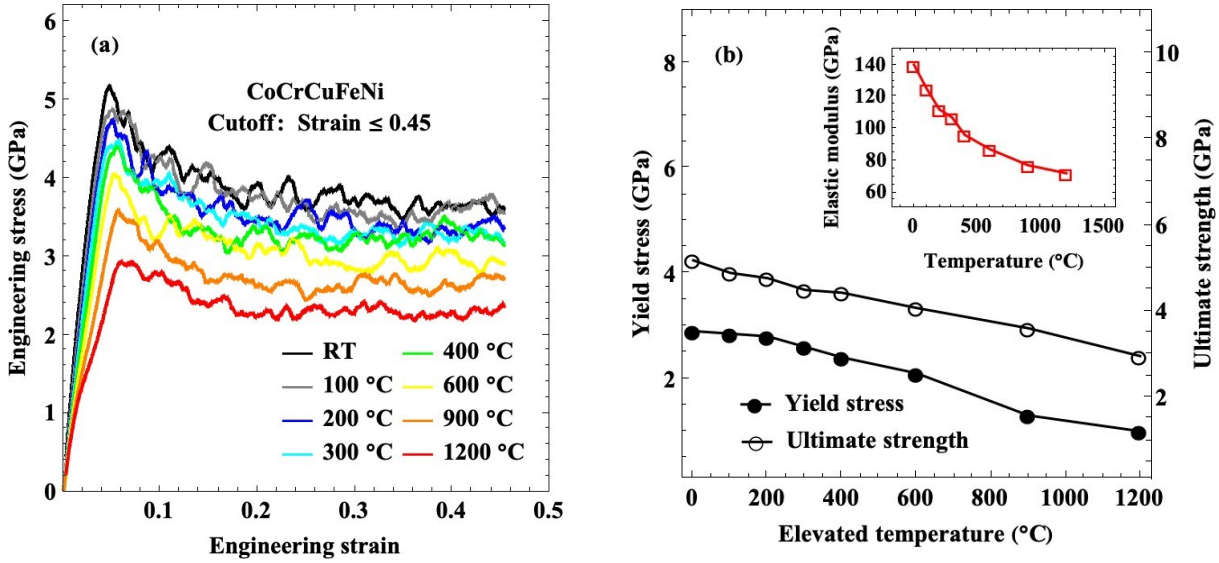

Fig. 2 Resulted mechanical properties of CoCrCuFeNi HEA at elevated temperatures, (a) engineering stress−strain curves, and (b) evolution of measured mechanical properties (Inset: evolution of elastic modulus).

3.2 Phase transformation

The CNA approach is one of the best ways to predict the phase transformation process during tensile deformation. Figure 3 observed the phase structures such as FCC, HCP, and others to understand the deformation-induced phase transformation process at high temperature. Percentage fractions (%) for phases were plotted as a function of tensile ε. Figure 3 (a) shows the evolution of FCC, HCP and others at RT, where others include any defects such as grain boundaries, voids, nano-angstrom cracks, dislocations and unknown structural mismatch. In the initial model after energy minimization, the FCC phase reaches 90%, and there are few HCP phases less than 0.1 %. Applying tensile deformation at RT decreases the FCC phase and increases the HCP phase. The deformation-induced phase transformation of metals in the FCC phase shows FCC→HCP transformation with a high probability and is accompanied by the generation and movement of partial dislocations (Olson and Cohen, 1976). In addition, in CoCrFeMnNi (Qi et al., 2021) and AlCoCrFeNi (Yoon et al., 2023) HEAs, it has been confirmed that a very small amount of BCC is generated at the tip of the FCC→HCP transformation. However, this phenomenon has not been found in the present CoCrCuFeNi HEA. This HEA contains Cu of 20 %, and it can be atomistically arranged with low strain energy with high ductility, so that it plays a role in minimizing the deformation energy during the deformation-induced phase transformation process. Thus, there is no occurrence of partial BCC at phase transformation tip of FCC→HCP. Further, the evolution of each phase transformation at elevated temperatures is plotted in both Fig. 2 (b) for FCC and Fig. 2 (c) for HCP. The FCC phase shows little change below 600 ℃, but a sharp decrease as the temperature above 600 ℃ rises. This reduction is almost determined in small deformation in the elastic and quasi-plastic regimes (less than the ε of 0.1) and has slight effect in large deformation beyond that. Conversely, the case of the HCP phase increases in the elastic and quasi-plastic regimes. The effect of elevated temperatures decreases as that of the FCC phase. Another thing is that the tendency of HCP phase to increase in the elastic and quasi-plastic regimes remains at 900 ℃. In other words, the effect of temperature greatly affects the FCC→HCP transformation, which greatly contributes to the tensile properties of this material shown in Fig. 2. On the other hand, the FCC→HCP transformation decreases near the yield point ($\varepsilon = 0.05$) as the temperature increases, and rather is damage could be caused by the increase in others such as grain boundaries and voids (Fig. 3 (d)). It affects the nonlinear reduction of E, as shown in Fig. 2 (b). In summary, as the temperature increases, the volume defect plays an important role rather than the phase transformation.

ISSN NO: 9726-001X
Volume 9 Issue 03 2021

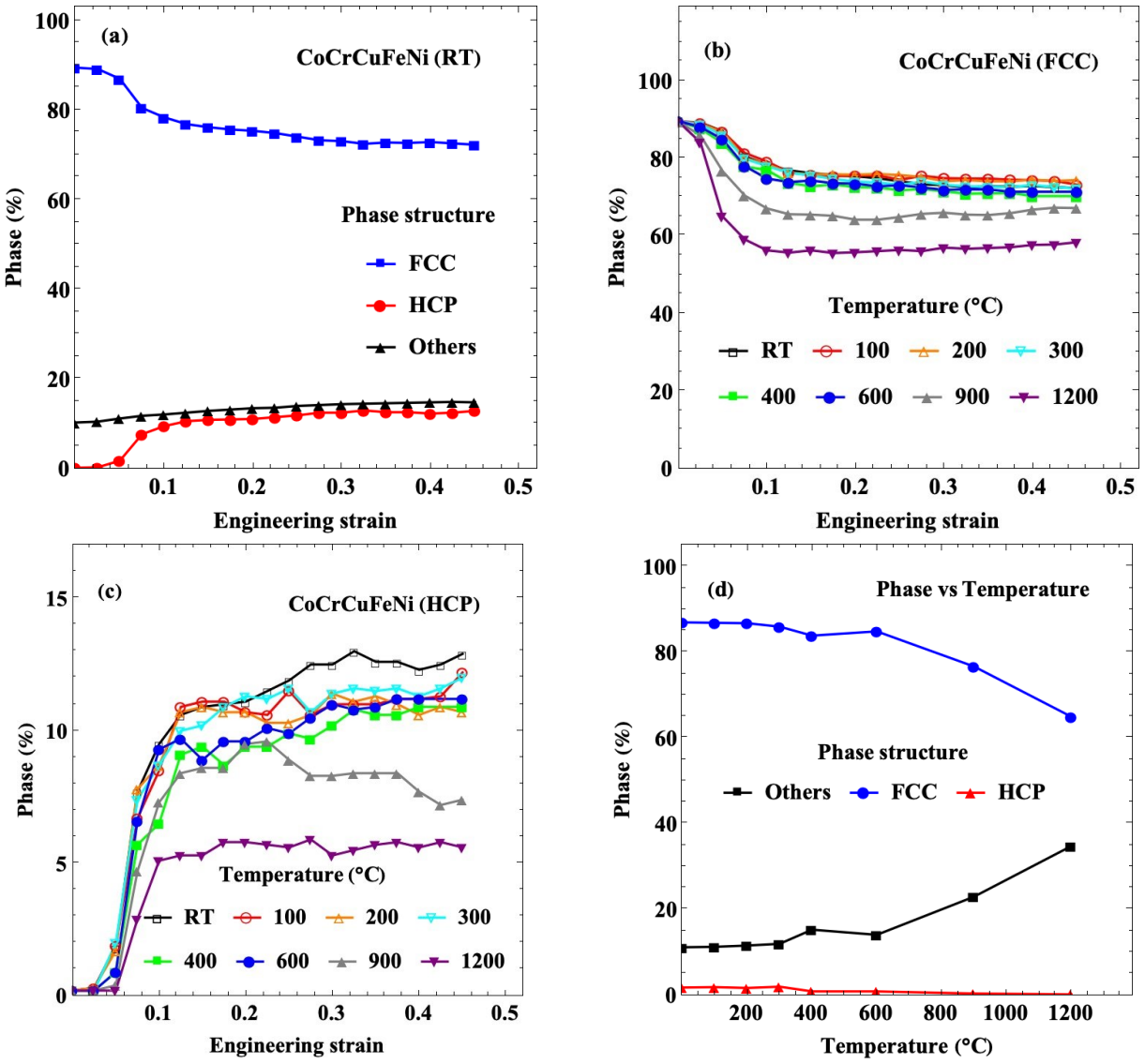

Fig. 3 Deformation-induced phase (FCC, HCP and others) transformation of CoCrCuFeNi HEA, (a) room temperature, (b) FCC at elevated temperatures, (c) HCP at elevated temperatures, and (d) phase transformation versus elevated temperature at $\varepsilon = 0.05$.

Figure 4 shows snapshots of the deformation-induced phase transformation of this material at RT. The variations of the FCC and HCP in the vicinity of the yield point ($\varepsilon = 0.04$) (Fig. 4 (b and d)) and the quasi-plastic regime ($\varepsilon = 0.08$) (Fig. 4 (c and e)) are shown as snapshots compared to the deformation-free state of $\varepsilon = 0$ (Fig. 4 (a)). We assumed that $\varepsilon = 0.04$ indicates the deformation within the elastic regime and $\varepsilon = 0.08$ indicates the deformation within the quasi-plastic regime. It was simplified to present different tensile curves based on the corresponding microstructure at different temperatures. This assumption remains the same under further microstructure observations. Figure 4 (b) shows how the HCP phase propagates (1→2). It is completely transformed for approximate deformation of $\varepsilon = 0.05$ from one GB to the other GB. This means that the deformation energy required for a bundle of HCP bands to be phase-transformed is not significant. Nevertheless, these HCP transformations show a numerous increase as they deform (Fig. 4 (c)). The creation or increase of other phases, such as BCC, was rarely found. In addition, as shown in Fig. 4 (d), the FCC→HCP phase transformation is performed without any segregation or aggregation of elements. This pattern is also the case in the quasi-plastic regime of Fig. 4 (e).

ISSN NO: 9726-001X
Volume 9 Issue 03 2021

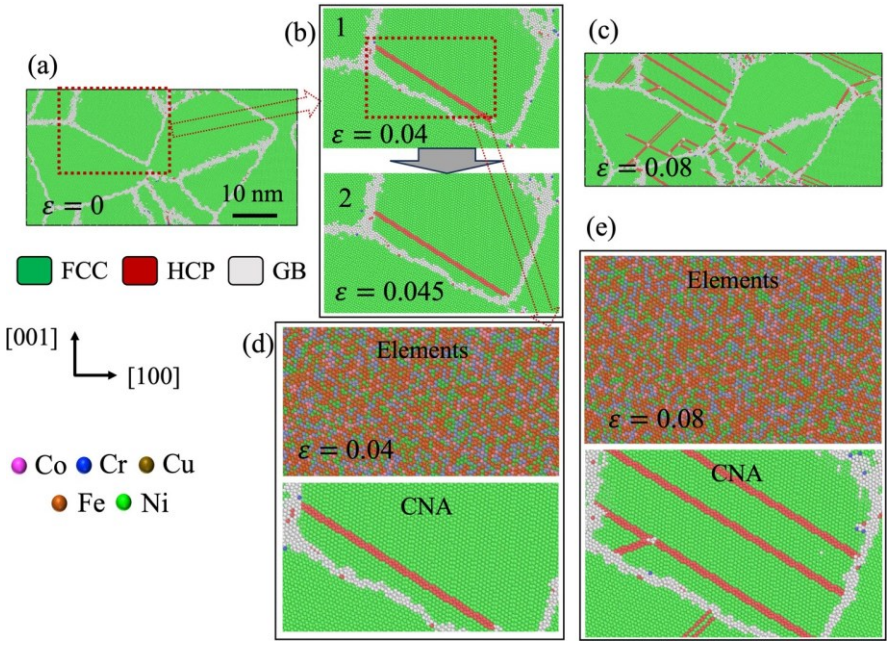

Fig. 4 Snapshots of deformation-induced phase transformation of CoCrCuFeNi HEA at room temperature, (a) ε =0, (b) band extension of HCP phase through 1 (ε =0.04) and 2 (ε =0.045), (c) that of ε =0.08, (d) comparison of elemental location and HCP phase at ε = 0.04, and (e) that at ε = 0.08.

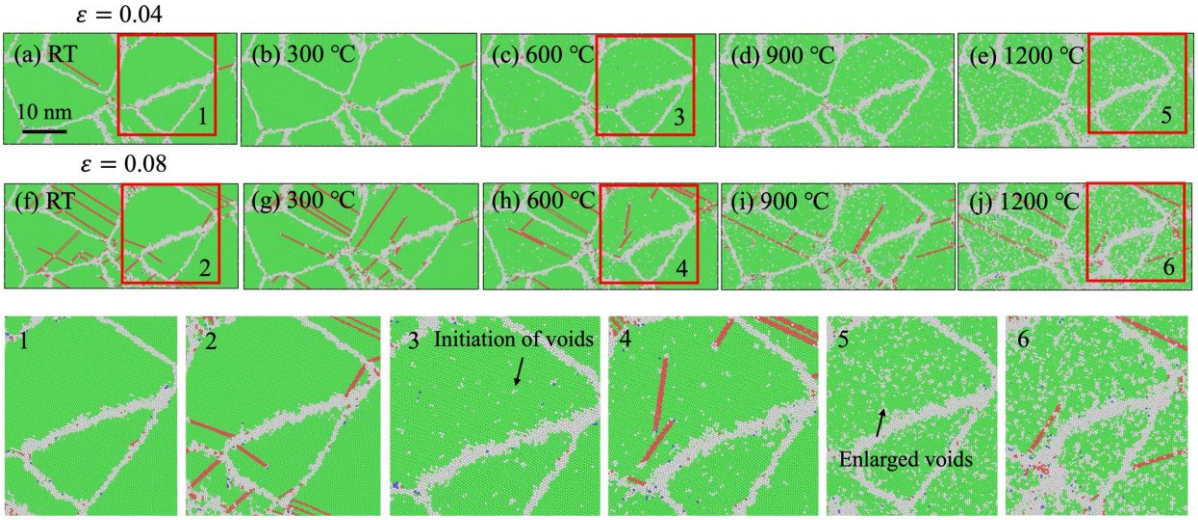

Fig. 5 Snapshots of nanostructure observation in the vicinity of the yield point (ε = 0.04) and the quasi-plastic regime (ε = 0.08) at elevated temperatures, (a-e) CNA in ε = 0.04 at RT, 300, 600, 900, and 1200 °C, (f-j) that in ε = 0.08 and (1-6) enlarged snapshots of (a), (c), (e), (f), (h), and (j).

Figure 5 shows snapshots of observed nanostructures in the vicinity of the yield point (ε = 0.04) and the quasi-plastic regime (ε = 0.08) at elevated temperatures. In Fig. 5 (a-e), the results in CNA in ε = 0.04 at RT, 300, 600, 900, and 1200 °C display that FCC→HCP phase transformation decreases as the temperature increases. On the other hand, the initiation of voids is observed at about 600 °C (Fig. 5 (c) and 3) compared to that at RT (Fig. 5 (a) and 1), which increases in size and number as the temperature increases (Fig. 5 (e) and 5). This phenomenon is the same in Fig. 5 (f-j). The deformed HCP in the quasi-plastic regime is more than that in the elastic regime, but it decreases as the temperature rises. This means that the FCC→HCP phase transformation is highly dependent on temperature. As shown in Fig. 3 (c), even by quantitative evaluation, there is no change in HCP phase even in the elastic regime as the temperature rises, but it changes very increasingly as it enters the plastic regime. Even the initiation and growth of voids as shown in (Fig. 5 (f, h, and j) and 2, 4, and 6) is similarly displayed as seen near the yield point (ε = 0.04).

ISSN NO: 9726-001X
Volume 9 Issue 03 2021

3.3 Dislocation evolution

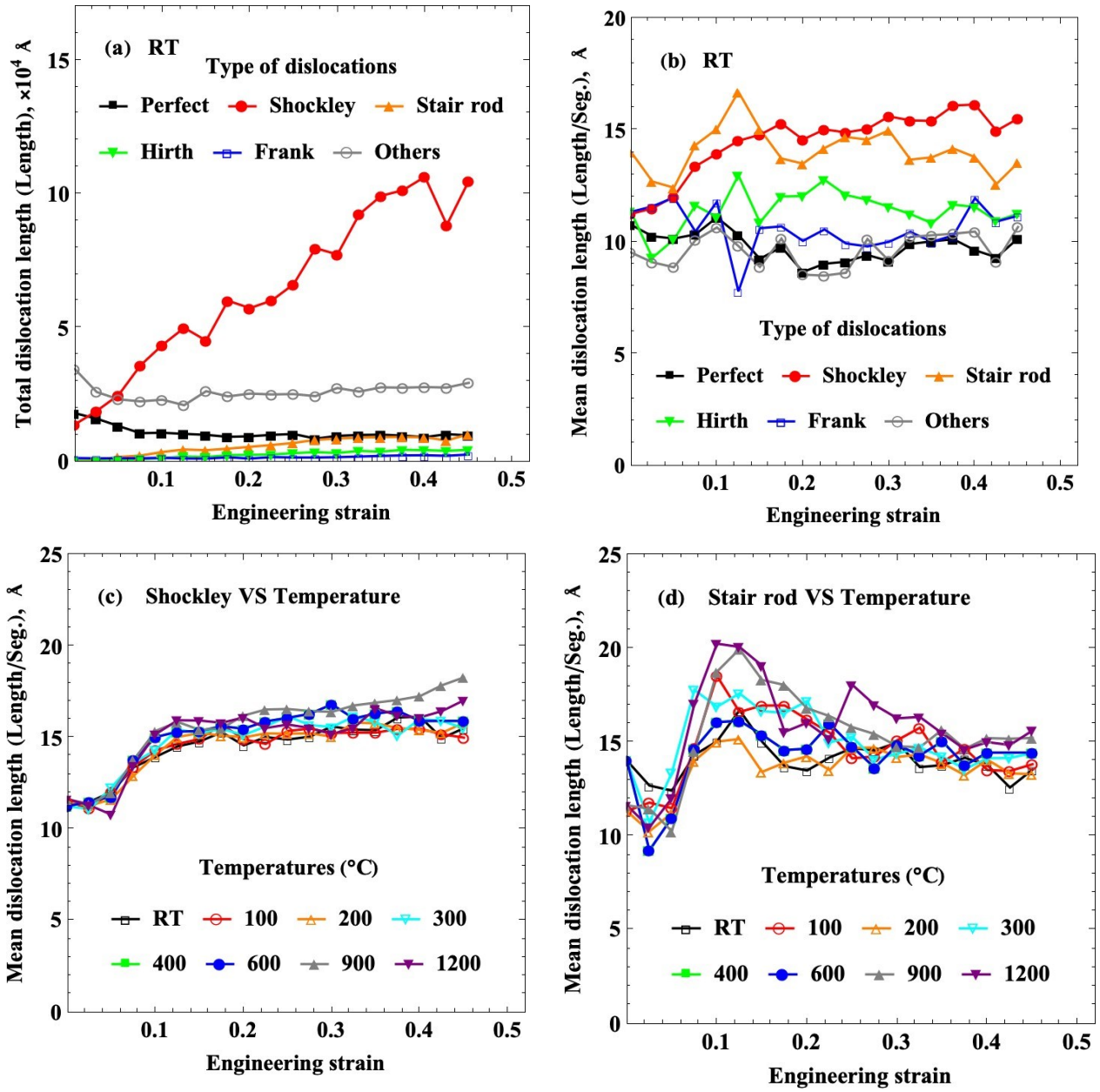

Fig. 6 Deformation-induced dislocation evolutions of CoCrCuFeNi HEA at room temperature and elevated temperatures, (a) evolution of total length for all possible dislocations at room temperature, (b) that of mean dislocation length at room temperature, (c) evolution of Shockley partial dislocation at elevated temperatures, and (d) that of stair-rod partial dislocation.

In Fig. 6, the deformation-induced dislocation evolutions of CoCrCuFeNi HEA were plotted. Figure 6 (a) shows the evolution of total length (unit: Å) for all possible dislocations at room temperature, and Figure 6 (b) is that of mean dislocation length at room temperature. The types of dislocations that can be generated during the tensile deformation process of this material were distinguished into perfect, Shockley, stair-rod, Hirth, Frank, and others representing certain structural defects. As shown in Fig. 6 (a), in the case of Shockley partial dislocations, the increase in the total dislocation length due to tensile deformation is very steep. The increase in stair-rod partial dislocations is also confirmed, but the increase in total dislocation length is overwhelmingly compared to the change in Shockley partial dislocation. Figure 6 (b) shows the total dislocation length of each type divided by the number of each (total dislocation length/the number of segments). We assume that it means the mean length of one dislocation. As a result, Shockley partial dislocation also shows a gradual increase in the elastic and quasi-plastic regimes, but the remaining other dislocations show an arbitrary

ISSN NO: 9726-001X
Volume 9 Issue 03 2021

pattern of repeating the increase and decrease. Only the Shockley partial dislocation extends longitudinally in a form in which the mean length increases based on a dislocation. Consequently, this phenomenon mainly contributes to determining the tensile properties of the material. In Fig. 6 (c), it shows the temperature dependence of the Shockley partial dislocation in tensile deformation. As a result, the Shockley partial dislocation is not significantly influenced by the elevated temperature. Even at extremely high temperatures above 900 ℃, there is no significant change. Therefore, Shockley partial dislocation is not involved in the change of tensile properties according to the elevated temperatures. In Fig. 6 (d), the evolution of stair-rod partial dislocation at the elevated temperatures is plotted. In the case of stair-rod partial dislocation, as in Shockley partial dislocation, there is no significant change in the elevated temperatures.

Figure 7 shows an example of how the Shockley partial dislocation does not have temperature dependence. Figure 7 (a) shows the partial dislocations near the yield point at RT. Parallel dislocations caused by tensile deformation are shown, and the dislocations are formed alternately between Shockley and Perfect. As shown in Fig. 7 (b-e), even if the temperature rises, the overall tendency is maintained without dislocation motion. This is consistent with the conclusion in Fig. 6 (c). As illustrated in Figs. 3 and 4, the effect of temperature on the tensile properties of this material can be described as the difference in the phase transformation process mainly due to the elevated temperatures.

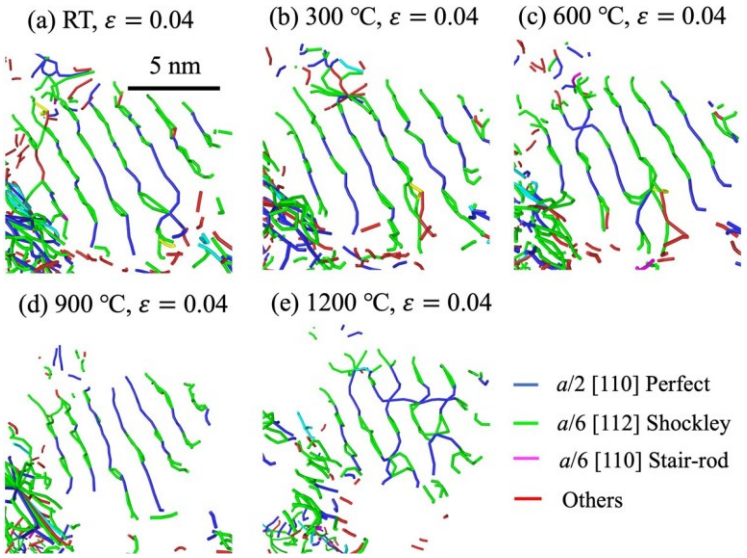

Fig. 7 Detailed snapshots of partial dislocations at elevated temperatures, (a) partial dislocations inside a grain at room temperature, (b) that of 300, (c) that of 600, (d) that of 900, and (e) that of 1200 ℃.

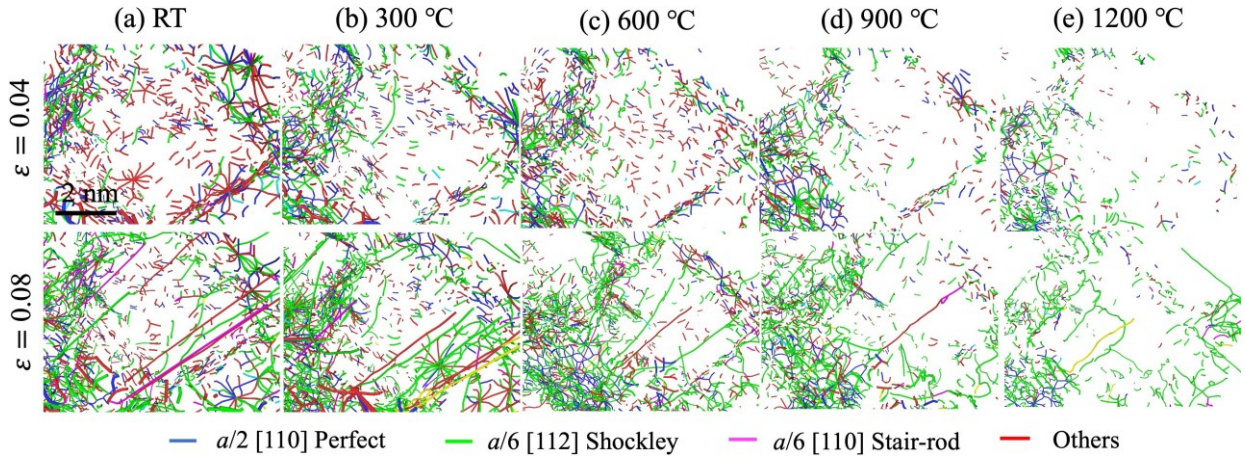

Fig. 8 Detailed snapshots in the stair-rod partial dislocation in the elastic regime of $\varepsilon = 0.04$ and the quasi-plastic regime of $\varepsilon = 0.08$, (a) partial dislocations inside a grain at room temperature, (b) that of 300, (c) that of 600, (d) that of 900, and (e) that of 1200 ℃.

Figure 8 shows the changes in the stair-rod partial dislocation in the elastic regime of $\varepsilon = 0.04$, which is near the yield point, and the quasi-plastic regime of $\varepsilon = 0.08$. Compared to the observation at RT, Fig. 8 (a), the stair-rod partial dislocation decreases as the temperature rises at $\varepsilon = 0.04$ (Fig. 8 (b-e)). On the other hand, in the quasi-plastic regime of $\varepsilon = 0.08$, the coupling and extension of the partial dislocations were confirmed. This phenomenon confirms the conclusion that the mean length (total length of dislocations/the number of segments) does not decrease even though the number of partial dislocations decreases. In addition, as the temperature goes higher, only the Shockley partial dislocation survives, and the other dislocations diffuse and disappear. Therefore, the distribution of partial dislocations as shown in Fig. 6 is confirmed, and it does not play a key role in determining tensile properties.

4. Conclusions

Thanks to nanostructure study by MD simulation based on phase and dislocation analysis, the high-temperature tensile characteristics of nanostructured polycrystalline CoCrCuFeNi HEA were grasped. The high temperature acceptability limit of this material under tensile loading is determined by the findings of this MD simulation. Here are the simulated findings that this investigation uncovered:
When the temperature is raised, the yield stress and ultimate tensile strength drop in a quasi-linear fashion, according to the engineering stress-strain curve. Nevertheless, there is a non-linear trend to the decline in elastic modulus. The high-temperature tensile characteristics of a material are determined by its deformation process in the elastic and quasi-plastic regimes. An immediate drop in elastic modulus at high temperatures is prevented by the phase structure (FCC→HCP) and activated partial dislocation (mostly stair-rod) that undergo nonlinear changes over 600 ℃. Extending the usefulness of CoCrCuFeNi HEA as a high-temperature material, it clarifies how the material resists thermal deterioration by keeping its elastic modulus even when heated.
2. The CNA findings demonstrated that the phase change process was brought about by tensile stress at high temperatures. We have identified the FCC→HCP phase transition as a prominent effect, which has been documented in previous HEAs. This material did not include BCC, which is often found near the tip of a phase transition. Thus, the primary function of deformation-induced phase change in the tensile characteristics of this material may be considered.

It was shown that FCC→HCP decreased as the temperature rose, and phase change due to tensile deformation had little bearing on elemental movement. Rather, it causes thermal degradation, which in turn reduces tensile characteristics as voids accumulate. It is evident that the phase shift from FCC to HCP and the creation of voids, which contribute to the tensile properties competitively, have been validated. A decrease in the FCC→HCP phase transition causes the elastic modulus to become insensitive. An essential factor is the fact that, as temperature rises, the proportion of volume defects, including voids and grain boundaries, increases.

4. DXA analysis was used to investigate several dislocation types, including perfect, Shockley, and stair-rod. In addition to

Tensile deformation has a strong influence on them, Shockley, and stair-rod dislocations; however, temperature elevation has little bearing on these parameters. We may say that deformation-induced phase transition is the major reason why the high-temperature tensile characteristics of this material are temperature dependent.

This investigation looked at the material's tensile characteristics when subjected to high temperatures. Phase change, which is crucial for high temperature tensile characteristics, was discovered to have taken place in this material using dislocation analysis and deformation-induced phase transition. Temperature dependence under tensile deformation, on the other hand, would not be affected by dislocation movements. This study's findings assess the material's potential for high-temperature applications; taken together, they suggest that, in uniaxial tensile mode, the material's high-temperature usage may be predicted by the gradual decrease of mechanical properties from room temperature up to 1200 ℃. In addition, by validating these predictions, the work proposes an optimisation method for high-temperature HEA applications and paves the way for the prediction of high-temperature tensile characteristics of additional nanostructured polycrystalline HEAs.

Acknowledgment

The authors would like to acknowledge "*Furo*" at Nagoya University Information Center, Japan, for providing the computational resources for this research. This work was supported by the JSPS KAKENHI (Grant-in-Aid for Early-Career Scientists, 23K13218) and also supported by the JSPS KAKENHI (Grant-in-Aid for Scientific Research (B) 23H01300).

References

Caro, A., and Farkas, D., Model interatomic potentials and lattice strain in a high-entropy alloy, Journal of Materials Research, Vol. 33 (2018), pp. 3218–3225.

Cantor, B., Chang, I. T. H., Knight, P., and Vincent, A. J. B., Microstructural Development in Equiatomic Multicomponent Alloys, Materials Science and Engineering: A, Vol. 375–377 (2004), pp. 213–218.

Deluigi, O. R., Pasianot, R. C., Valencia, F. J., Caro, A., Farkas, D., and Bringa, E. M., Simulations of Primary Damage in a High Entropy Alloy: Probing Enhanced Radiation Resistance, Acta Materialia, Vol. 213 (2021), pp. 116951 (1–10).

Fujii, T., Suzuki, M., and Shimamura, Y., Susceptibility to Intergranular Corrosion in Sensitized Austenitic Stainless Steel Characterized via Crystallographic Characteristics of Grain Boundaries, Corrosion Science, Vol. 195 (2022), pp. 109946 (1–10).

Hirano, A., Sakakima, H., Hatano, A., and Izumi, S., Reaction Pathway Analysis for the Contraction of 4H-SiC Partial-Dislocations Pair in the Vicinity of Surface, Japanese Journal of Applied Physics, Vol. 60, No. 8 (2021), pp. 085502 (1–8).

Hirel, P., Atomsk: A Tool for Manipulating and Converting Atomic Data Files, Computer Physics Communications, Vol. 197 (2015), pp. 212–219.

Laplanche, G., Gadaud, P., Horst, O., Otto, F., Eggeler, G., and George, E. P., Temperature Dependencies of the Elastic Moduli and Thermal Expansion Coefficient of an Equiatomic, Single-Phase CoCrFeMnNi High-Entropy Alloy, Journal of Alloys and Compounds, Vol. 623 (2015), pp. 348–353.

Muskeri, S., Hasannaeimi, V., Salloom, R., Sadeghilaridjani, M., and Mukherjee, S., Small-Scale Mechanical Behavior of a Eutectic High Entropy Alloy, Scientific Reports, Vol. 10, No. 1 (2020), pp. 2669 (1–12).

Olson, G. B., and Cohen, M., A General Mechanism of Martensitic Nucleation: Part I. General Concepts and the FCC->HCP Transformation, Metallurgical and Materials Transactions A, Vol. 7, No. A (1976), pp. 1897–1904.

Park, N., Watanabe, I., Terada, D., Yokoyama, Y., Liaw, P. K., and Tsuji, N., Recrystallization Behavior of CoCrCuFeNi High-Entropy Alloy, Metallurgical and Materials Transactions A, Vol. 46, No. 4 (2015), pp. 1481–1487.

Plimpton, S., Fast Parallel Algorithms for Short-Range Molecular Dynamics, Journal of Computational Physics, Vol. 117 (1995), pp. 1–19.

Praveen, S., and Kim, H. S., High-Entropy Alloys: Potential Candidates for High-Temperature Applications–An Overview, Advanced Engineering Materials, Vol. 20, No. 1 (2018), pp. 1700645 (1–22).

Qi, Y., Zhao, M., and Feng, M., Molecular Simulation of Microstructure Evolution and Plastic Deformation of Nanocrystalline CoCrFeMnNi High-Entropy Alloy under Tension and Compression, Journal of Alloys and Compounds, Vol. 851 (2021), pp. 156923 (1–9).

Senkov, O. N., Wilks, G. B., Scott, J. M., and Miracle, D. B., Mechanical Properties of $Nb_{25}Mo_{25}Ta_{25}W_{25}$ and $V_{20}Nb_{20}Mo_{20}Ta_{20}W_{20}$ Refractory High Entropy Alloys, Intermetallics, Vol. 19, No. 5 (2011), pp. 698–706.

Seoane, A., Farkas, D., and Bai, X.-M., Molecular Dynamics Studies of Sluggish Grain Boundary Diffusion in Equiatomic FeNiCrCoCu High-Entropy Alloy, Journal of Materials Science, Vol.58, No. 21 (2023), pp. 8845–8861.

Shams, S. A. A., Jang, G., Won, J. W., Bae, J. W., Jin, H., Kim, H. S., and Lee, C. S., Low-Cycle Fatigue Properties of CoCrFeMnNi High-Entropy Alloy Compared with Its Conventional Counterparts, Materials Science and Engineering: A, Vol. 792 (2020), pp. 139661 (1–11).

Shirasu, K., Kitayama, S., Liu, F., Yamamoto, G., and Hashida, T., Molecular Dynamics Simulations and Theoretical Model for Engineering Tensile Properties of Single-and Multi-Walled Carbon Nanotubes, Nanomaterials, Vol. 11, No. 3 (2021), pp. 795 (1–10).

Stukowski, A., Visualization and Analysis of Atomistic Simulation Data with OVITO–the Open Visualization Tool, Modelling and Simulation in Materials Science and Engineering, Vol. 18, No. 1 (2010), pp. 015012 (1–7).

Suzuki, S., Sakaguchi, M., and Inoue, H., Temperature Dependent Fatigue Crack Propagation in a Single Crystal Ni-Base Superalloy Affected by Primary and Secondary Orientations, Materials Science and Engineering: A, Vol. 724 (2018), pp. 559–565.

Suzuki, K., Koyama, M., Hamada, S., Tsuzaki, K., and Noguchi, H., Planar Slip-Driven Fatigue Crack Initiation and Propagation in an Equiatomic CrMnFeCoNi High-Entropy Alloy, International Journal of Fatigue, Vol. 133 (2020), pp. 105418 (1–10).

Suzuki, S., Sakaguchi, M., Domen, M., Karato, T., and Suzuki, K., Temperature and ΔK Dependence of Grain Boundary Effect on Fatigue Crack Propagation in a Two-Dimensional Polycrystalline Ni-Base Superalloy, Acta Materialia, Vol. 240 (2022), pp. 118288(1–14).

Varshni, Y. P., Temperature Dependence of the Elastic Constants, Physical Review B, Vol. 2, No. 10 (1970), pp. 3952–3958.

Voronoi, G., Nouvelles applications des paramètres continus à la théorie de formes quadratiques, Journal für die reine und angewandte Mathematik, Vol. 134 (1908), pp. 198–287.

Xiao, Y., Zou, Y., Ma, H., Sologubenko, A. S., Maeder, X., Spolenak, R., and Wheeler, J. M., Nanostructured NbMoTaW High Entropy Alloy Thin Films: High Strength and Enhanced Fracture Toughness, Scripta Materialia, Vol. 168 (2019), pp. 51–55.

Yeh, J.-W., Chen, S.-K., Lin, S.-J., Gan, J.-Y., Chin, T.-S., Shun, T.-T., Tsau, C.-H., and Chang, S.-Y., Nanostructured High-Entropy Alloys with Multiple Principal Elements: Novel Alloy Design Concepts and Outcomes, Advanced Engineering Materials, Vol. 6, No. 5 (2004), pp. 299–303.

Yoon, S., Kimura, Y., Gu, S., Toku, Y., Ju, Y., and Cui, Y., Thermal Stress-Assisted Formation of Submicron Pillars from a Thin Film of CoCrCuFeNi High Entropy Alloy: Experiments and Simulations, RSC Advances, Vol. 13, No. 41(2023), pp. 28513–28526.

Yoon, S., Kimura, Y., Uchida, M., Ju, Y., and Toku, Y., High Temperature Tensile and Compressive Behaviors of Nanostructured Polycrystalline AlCoCrFeNi High Entropy Alloy: A Molecular Dynamics Study, Journal of Engineering Materials and Technology, Vol. 146, No. 2 (2024), pp. 021003(1–11).

Zou, Y., Nanomechanical Studies of High-Entropy Alloys, Journal of Materials Research, Vol. 33, No. 19 (2018), pp. 3035–3054.